ACS APPLIED MATERIALS & INTERFACES

Research Article

www.acsami.org

Silver Alginate Hydrogel Micro- and Nanocontainers for Theranostics: Synthesis, Encapsulation, Remote Release, and Detection

Ekaterina Lengert,[*,†,‡] Mariia Saveleva,[†,‡] Anatolii Abalymov,[†] Vsevolod Atkin,[†] Pieter C. Wuytens,[‡,§] Roman Kamyshinsky,[∥,▽] Alexander L. Vasiliev,[∥,⊥] Dmitry A. Gorin,[†] Gleb B. Sukhorukov,[#] Andre G. Skirtach,[‡] and Bogdan Parakhonskiy[‡,⊥]

[†]Department of Nano- and Biomedical Technologies, Saratov State University, Astrakhanskaya 83, 410012 Saratov, Russia

[‡]Department of Molecular Biotechnology, Ghent University, Coupure Links 653, 9000 Gent, Belgium

[§]Photonics Research Group, INTEC Department, Ghent University - imec, Technologiepark 15, 9052 Zwijnaarde, Belgium

[∥]National Research Center, Kurchatov Institute, Akademika Kurchatova pl., 1, 123182 Moscow, Russia

[⊥]A.V. Shubnikov Institute of Crystallography, Russian Academy of Science, Leninskiy prospect, 59, 119333 Moscow, Russia

[#]School of Engineering and Materials Science, Queen Mary University of London, Mile End Road, London, E1 4NS, U.K.

[▽]Moscow Institute of Physics and Technology, Institutsky lane 9, Dolgoprudny, 141700 Moscow region, Russia

Supporting Information

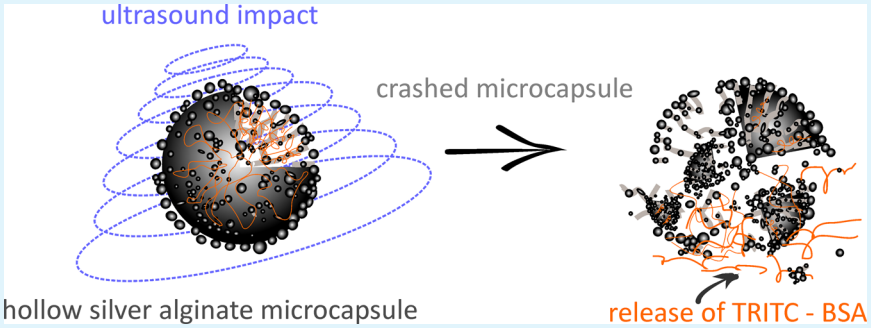

ABSTRACT: We have designed multifunctional silver alginate hydrogel microcontainers referred to as loaded microcapsules with different sizes by assembling them via a template assisted approach using natural, highly porous calcium carbonate cores. Sodium alginate was immobilized into the pores of calcium carbonate particles of different sizes followed by cross-linking via addition of silver ions, which had a dual purpose: on one hand, the were used as a cross-linking agent, albeit in the monovalent form, while on the other hand they have led to formation of silver nanoparticles. Monovalent silver ions, an unusual cross-linking agent, improve the sensitivity to ultrasound, lead to homogeneous distribution of silver nanoparticles. Silver nanoparticles appeared on the shell of the alginate microcapsules in the twin-structure as determined by transmission electron microscopy. Remote release of a payload from alginate containers by ultrasound was found to strongly depend on the particle size. The possibility to use such particles as a platform for label-free molecule detection based on the surface enhanced Raman scattering was demonstrated. Cytotoxicity and cell uptake studies conducted in this work have revealed that microcontainers exhibit nonessential level of toxicity with an efficient uptake of cells. The above-described functionalities constitute building blocks of a theranostic system, where detection and remote release can be achieved with the same carrier.

KEYWORDS: *silver alginate hydrogel micro- and nanocontainers, encapsulation, ultrasound-induced release, silver nanoparticles, SERS, cell uptake*

INTRODUCTION

At the present time, an actual challenge of biomedicine is the creation of materials and structures which provide targeted delivery of drugs[1] in combination with the possibility of diagnostics, remote control, monitoring, and release of biologically active agents. Unfortunately, there is a limited number of delivery structures which allow the combination of detection of biological marker and release of medicines depending on concentration of biological markers. Materials which are based on organic−inorganic hybrid systems composed of hydrogel and inorganic nanoparticles have attracted significant attention by virtue of their combined physicochemical properties and rapidly

Received: June 7, 2017
Accepted: June 12, 2017
Published: June 12, 2017

DOI: 10.1021/acsami.7b08147
ACS Appl. Mater. Interfaces 2017, 9, 21949−21958

become a new fascinating class of materials.[2] One of main tasks consists of the fabrication of intelligent micro- and nano-sized biocompatible containers that protect contents and provide a release at the designated place and at a desired time point.

A theranostic object needs to provide the possibility to encapsulate and release drugs[3,4] as well as to possess appropriate detection capabilities of biological markers by surface enhanced Raman spectroscopy (SERS).[5,6] A number of appropriate delivery carriers has a limit.[2] In this regard, their modification of delivery containers with silver nanoparticles makes possible to change optical properties of microcontainers,[7−9] to accomplish the detection of substances by using surface enhanced Raman scattering (SERS),[10−12] to enhance mechanical characteristics of the material,[13] and to increase its sensitivity to ultrasonic exposure by controlling the density of the shell.[14] Due to its antiseptic properties, silver nanoparticles possess antimicrobial[15−18] and antibacterial properties,[19−21] and its incorporation into microcapsules opens prospects for their application in medicine.

The release of encapsulated agents is possible by using an enzymatic degradation of hollow capsules[22,23] manipulation of the charge of the capsule surface,[24] pH,[25−28] and release mechanisms based on recrystallization.[29,30] Ultrasound has been used to trigger release of encapsulated material from polyelectrolyte multilayer capsules.[31−36] It was found that the permeability and integrity of the capsule shell depend on the density of the carrier as well as on the power density, frequency, and duration of ultrasonic exposure.[14,37] Its capability to penetrate deep into tissue and a possibility of a targeted action make ultrasound a method of choice for application in medicine.[38] Clinically approved hardware is available, and a wide variety of parameters (frequencies ranging from 20 kHz to 3 MHz and intensities from a 0.1 to 100 W/cm^2) have been investigated for ultrasound stimulated drug release.[39] Recently, intensities of ultrasound necessary for release were achieved in the range of those allowed for medical applications.[40]

The size of particles is essential for in vivo applications[41,42] and, specifically, for theranostic applications.[43] In the latter case, particles at different sizes assembled into a multcompartment carrier were demonstrated.[44] Recently, we have introduced alginate based container formation,[45] but their essential functionalities, size adjustment, release methods, and shell structure suitable for release and detection have not been reported.

In this work, we investigate synthesis, realized size control of templates, and encapsulate molecules enabling their subsequent ultrasound stimulated release and detection of biologically relevant molecules. A template assisted technique was applied to produce highly porous calcium carbonate microparticles used as templates for fabrication of silver alginate hydrogel micro- and nanocontainers. Further, we investigate the encapsulation of fluorescently labeled bovine serum albumin as a model system and perform low-power ultrasound (allowed in medicine) stimulated remote release from alginate particles with different sizes. Detection of molecules was achieved by surface enhanced Raman scattering, where enhancement of the Raman signal was obtained by functionalizing the shell with silver nanoparticles. The presence of silver nanoparticles is also important for increasing the density of the shell functionality relevant for ultrasound action. As such, detailed analysis of the structures of silver nanoparticles was performed by high resolution electron microscopy.

EXPERIMENTAL SECTION

Materials and Reagents. Sodium alginate (ALG) $(C_6H_8O_6)_n$ (viscosity 15−20 cP, 1% in H_2O (lit.)), calcium chloride ($CaCl_2$), silver nitrate ($AgNO_3$), sodium carbonate (Na_2CO_3), ethylene glycol ($C_2H_6O_2$), ascorbic acid ($C_6H_8O_6$), and bovine serum albumin (BSA; TRITC 70 kDa) were purchased from Sigma-Aldrich. In all experiments, ultrapure water with resistivity higher than 18.2 MΩ cm was used.

Characterization. The following devices were used for $CaCO_3$ microparticles synthesis: the ultrasonic homogenizer Sonopuls (Bandelin, Germany) at the frequency of 20 kHz and power density of 1 W/cm^2 and magnetic stirrer MP Standart (IKA, Germany).

The ultrasonic bath (Sapfir, Russia) was used for ultrasound treatment of silver alginate microcapsules at 35 kHz frequency and power density 0.64 W/cm^2.

Particle morphology characterization was performed by using images obtained by scanning electron microscopy (SEM) and transmission/scanning transmission electron microscopy (TEM/STEM). SEM measurements were performed with MIRA II LMU (Tescan) at the operating voltage of 30 kV, in second electron and back scattering electron mode. Magnification was ranged from 100 to 40 000 times. Samples were prepared by drying a drop of the aqueous suspension of microcapsules on the silicon wafer.

The size distribution of the calcium carbonate particles was obtained by post processing and image analysis of SEM micrographs with ImageJ software (NIH, http://rsb.info.nih.gov/ij/). At least 100 measurements per sample were performed.

TEM/STEM study was performed in a Titan 80-300 TEM/STEM (FEI, USA), equipped with a Schottky field emission gun and energy dispersive X-ray spectroscopy system (EDXS; EDAX, USA). The research was carried out at 300 kV in STEM bright field (BF) mode and high resolution (HR) TEM. Samples were prepared by drying a drop of the aqueous suspension of microparticles on the copper grid. Size distribution of Ag nanoparticles was performed by post processing of the micrographs with Digital Micrograph (Gatan, USA) and TIA (FEI, USA) software.

The fluorescence imaging of hollow silver alginate microcapsules loaded TRITC−BSA was implemented by using a fluorescent confocal laser scanning microscope TCS SP8 (Leica, Germany). During the process of sample preparation for imaging, 5 μL of each sample, stained with the TRITC−BSA conjugation, was placed on a cover glass slip. The excitation wavelength is 552 nm, and the TRITC fluorescence was detected at wavelengths of 565 and 620 nm.

Particles Synthesis. Spherical calcium carbonate microparticles (with a mean diameter of 3.0 ± 0.3 μm) were synthesized via the protocol of Volodkin et al.[46] as follows: 1 mL of Na_2CO_3 (0.33 M) and 1 mL of $CaCl_2$ (0.33 M) were rapidly mixed in a glass vessel and stirred at 500 rpm for 1 min. The color of the mixture became white immediately after mixing. Precipitated microparticles of calcium carbonate ($CaCO_3$) were collected by centrifugation (2000 rpm, 2 min) and subsequently washed with pure ethanol. This procedure was repeated three times, and then microparticles were dried in an oven at 60 °C for 30 min.

The same procedure of $CaCO_3$ particle synthesis was used for the formation of calcium carbonate microparticles with the mean diameter of 1.0 ± 0.1 μm using the protocol described by Svenskaya et al.[47] briefly, but there is the only difference that stirring of the reaction mixture was carried out with ultrasound (US) with a frequency of 20 kHz and power density 1 W/cm^2 during 1 min.

For the formation of calcium carbonate microparticles with the mean diameter of 0.8 ± 0.2 μm the protocol developed by Parakhonskiy et al. was used.[30] In this case for synthesis the salts precipitation in dense media (ethylene glycol was used), in details 12 mL of salt solutions (water solutions of salt mixed with ethylene glycol with concentrations of 0.33 M and 83% respectively by a ratio of 1:5) were used.[30] The mixing process of two salt solutions was carried out by magnetic stirrer with a speed of 700 rotations/min for 3 h. After preparation of calcium carbonate microparticles, all samples were washed three times with ethanol using centrifugation with a speed of 3200 rotations/min for 5 min. The morphology of the obtained samples was observed by scanning electron microscopy (Figure 1).

DOI: 10.1021/acsami.7b08147
ACS Appl. Mater. Interfaces 2017, 9, 21949−21958

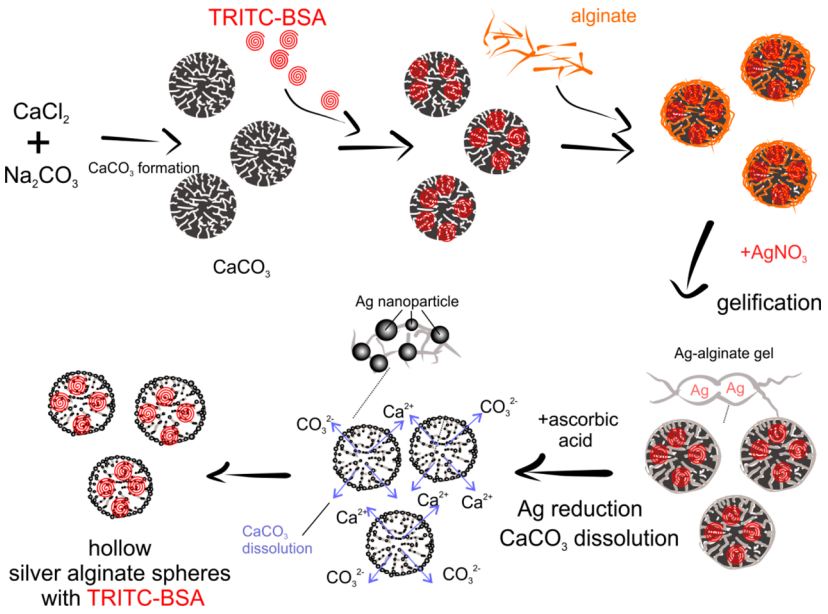

Figure 1. Scheme of the preparation of silver alginate hydrogel microcontainers.

Loading of $CaCO_3$ Particles with TRITC−BSA. The encapsulation of TRITC−BSA macromolecules into $CaCO_3$ microparticles was performed via adsorption method as follows: 20 mg of $CaCO_3$ microparticles powder was placed in a 2 mL plastic tube, and 0.5 mL of 1 mg/mL TRITC−BSA solution was added. This system was intensively shaken for 30 min. The microparticle suspension was centrifuged (2500 rpm, 2 min) and washed once with water. Finally, the collected microparticles with encapsulated TRITC−BSA were ready to be used for the fabrication of silver alginate microcontainers as mentioned above. The supernatants were collected for the following loading efficiency and capacity estimation.

Preparation of Hollow Silver Alginate Hydrogel Microcontainers. To produce silver alginate hydrogel microcontainers, 40 mg of $CaCO_3$ microparticles powder were placed in a 2 mL Eppendorf tube. A total of 1 mL of 5 mg/mL sodium alginate was injected into the tube and was left to agitate for 10 min in a shaker. After that, sodium alginate-coated $CaCO_3$ microparticles were washed three times by deionized water. Next, 0.5 mL of 0.75 M $AgNO_3$ was added to prepared in advance sodium alginate $CaCO_3$ microparticles in order to initiate cross-linking of sodium alginate. The mixture was agitated for 10 min in a shaker and subsequently thoroughly washed with deionized water. In the last step, 0.5 mL of 0.1 M ascorbic acid was added to microparticles for the gradual removal of the $CaCO_3$ core and growing of silver nanoparticles, yielding the hollow structure of the silver alginate hydrogel microcapsules. After that, microcontainers were collected by centrifugation and thoroughly washed with clean water. Hollow silver alginate hydrogel microcontainers were stored in water (Figure 1).

Raman Microscopy. Raman spectra were acquired on a WITec Alpha 300 R+ confocal Raman microscope equipped with a −70 °C cooled CCD camera (Andor iDus 401 BR-DD) and a 785 nm diode laser (Toptica, XTRA II). A monolayer of 4-nitrothiophenol (4-NTP, sigma) molecules was adsorbed on the silver surface, which serve as reporter molecules for quantifying the SERS substrate enhancement factor.[48] To this end, the microcapsules were incubated overnight in a 1 mM 4-NTP solution in ethanol. Next, the particles were washed four times (centrifugation for 3 min at 3000 rpm) with ethanol to remove excessive, nonbound molecules. Finally, the ethanol was replaced by DI water. SERS spectra were acquired using a Nikon PlanFluar 10×/0.3 objective, a laser power of 300 μW, and an integration time of 0.13. The spontaneous Raman scattering of a 50 mM 4-NTP solution in ethanol was measured using identical conditions but with a laser power of 100 mW. The effective height of the collection volume was measured to be 160 μm from an axial scan on a 50 nm thick TiO_2 layer deposited on a CaF substrate (Supporting Information, Figure S1).

Ultrasound Release. The release of TRITC−BSA, encapsulated in hollow silver alginate microcapsules, was stimulated by ultrasound treatment, which destroys alginate shells. In order to study the release process, 5 equal samples were prepared for each of three classes of microcapsules. A total of 1 mL of the silver alginate particle suspension (8 mg/mL) was placed into 2 mL Eppendorf microtubes. These microtubes were placed in an US bath, and US treatment of microcapsules was carried out (frequency 35 kHz and power density 0.64 W/cm^2). During this process, tubes were successively taken out from the bath at fixed time intervals (1, 15, 35, 45, 60, 120, and 180 min of treatment). This procedure was carried out for each independent sample and class of microcapsules. After the treatment the suspensions were centrifuged to obtain sediments, and the concentrations of the released substances were investigated in supernatant solution via spectrophotometry, and the number of destroyed microcapsules was investigated via scanning electron microscopy.

Loading Efficacy of Hollow Silver Alginate Microcontainers with TRITC−BSA. The loading efficacy of alginate microcapsules with TRITC−BSA was estimated using spectrophotometry Cary Eclipse (Varian, USA). For this the supernatants after microcapsules loading were collected in a separate tube and the absorbance at 556 nm wavelength of TRITC−BSA in its water solution was measured. The concentration and as a result the mass ($M_{supernatant}$) of free (non-encapsulated) TRITC−BSA were calculated based on the experimental calibration curve.

The loading capacity of microcapsules (W) was determined as the relation of the encapsulated substance mass ($M_{loading}$) on the corresponding mass of pure unloaded microparticles ($M_{particles}$):

$$W = \frac{M_{initial} - M_{supernatant}}{M_{particles}} = \frac{M_{loading}}{M_{particles}} \times 100\% \quad (1)$$

where $M_{initial}$ is the initial mass of the TRITC−BSA molecule, which was added to suspension for encapsulation.

Cell Preparation. HeLa cells were provided by the Department of Cell Engineering, Education and Research Institute of Nanostructures and Biosystems, Saratov State University, Russia. All cells were plated separately in tissue culture flasks and cultivated in Dulbecco's modified eagle medium (DMEM, Sigma-Aldrich), containing 10% fetal bovine serum (FBS, Hyclone), 2 mM L-glutamine (Sigma-Aldrich), and 1% penicillin-streptomycin antibiotic antifungal cocktail (Sigma-Aldrich). The medium was replaced every 3 days, and cells were maintained in a humidified incubator at 37 °C with 5% CO_2. Cell cultures with 75−85%

DOI: 10.1021/acsami.7b08147
ACS Appl. Mater. Interfaces 2017, 9, 21949−21958

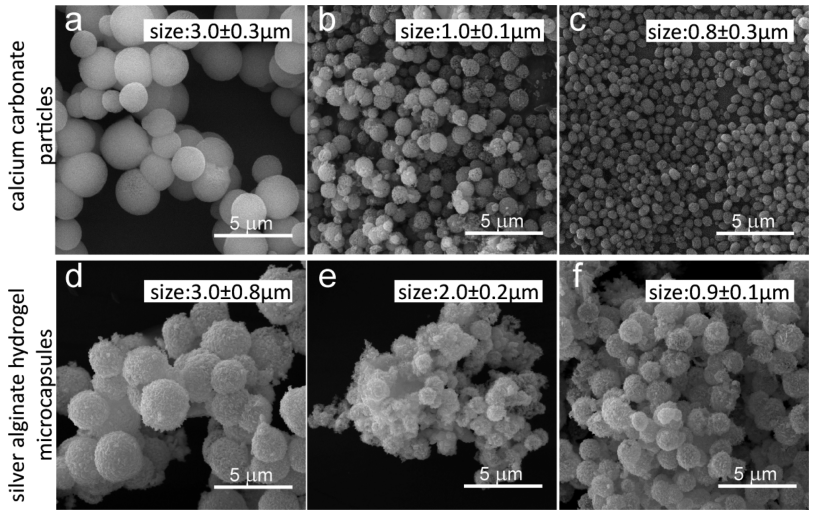

Figure 2. (a–c) SEM images of calcium carbonate and hollow silver alginate microcapsules synthesized with different methods: (a) using a magnetic stirrer, (b) ultrasound agitation, and (c) synthesis in ethylene glycol medium. Alginate microcapsules synthesized based on the corresponded template $CaCO_3$ particles: (d) calcium carbonate particles synthesized using a magnetic stirrer, (e) calcium carbonate particles synthesized under ultrasound agitation, and (f) calcium carbonate particles synthesized in ethylene glycol medium. The sizes of hollow silver alginate microcontainers are determined by templates.

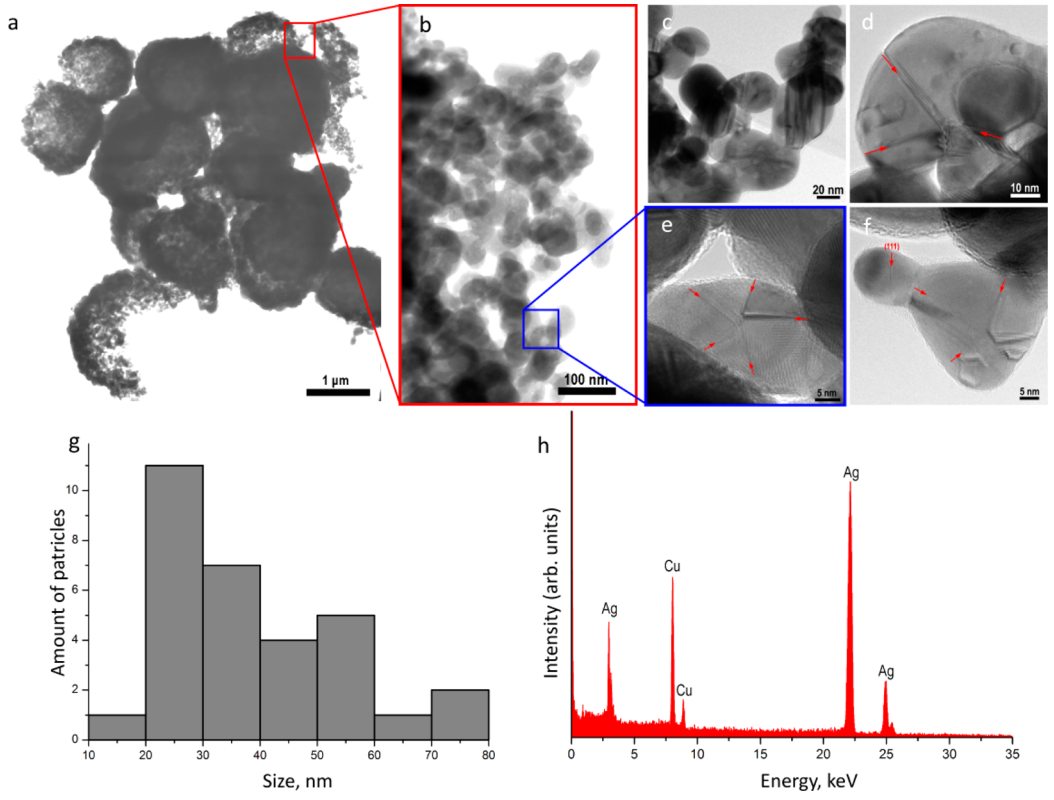

Figure 3. Images of the silver alginate microcapsules at different magnification: (a) BF STEM overview image of the hollow silver alginate microcapsules, (b) enlarged BF STEM image of silver nanoparticles, (c–f) HR TEM images of silver nanoparticles on silver alginate hydrogel shell with different magnifications, red arrows indicate twinning planes parallel to {111} crystal planes, (g) the size distribution of silver nanoparticles estimated from the images in panels b and c, and (h) results of EDXS analysis of the hollow silver alginate hydrogel microcapsules.

confluence were harvested using 0.25% trypsin (Life technologies) and counted with a hemocytometer.

All materials were sterilized with 70% ethanol for 30 min, air-dried, and washed three times with PBS. Then cells were seeded on the sample surfaces in DMEM cell culture medium with an average density 4×10^5. The samples were maintained in a CO_2 incubator overnight.

Cell Viability. HeLa cells were seeded into 96-well cell culture plates at a cell density of 10×10^4/well. After 24 h cultivation, samples 10×10 mm^2 were placed into the plate in the culture medium and incubated overnight at 37 °C under 5% CO_2. Subsequently, cells were incubated (Innova CO-170, New Brunswick Scientific) at 37 °C for 4 h, together with added materials. In the last step, 100 μL of fluorescence dye was added to each well (AlamarBlue, Sigma-Aldrich), and the fluorescent (540/610 nm) intensity was measured by a spectrophotometer (Synergy H1Multi-Mode Reader). The cell viability was studied for up to 3 days using the dye exclusion method.

DOI: 10.1021/acsami.7b08147
ACS Appl. Mater. Interfaces 2017, 9, 21949–21958

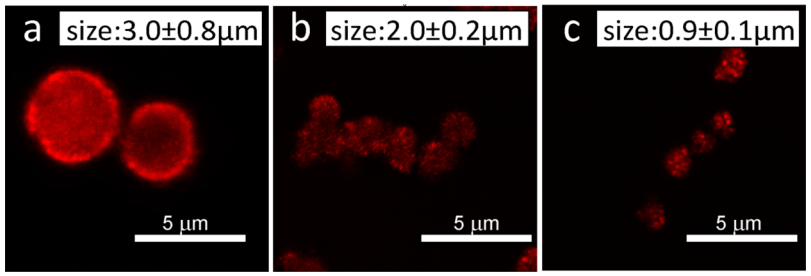

Figure 4. Confocal microscopy images of the silver alginate microcontainers with different sizes: (a) 3.0 ± 0.8, (b) 2.0 ± 0.2, and (c) 0.9 ± 0.1 μm.

Cellular Uptake. HeLa cells were added to five tissue culture dishes (5×10^5 cells/dish). After 24 h, cells were coincubated with hollow alginate silver microcontainers of three different sizes (labeled with a fluorescence dye tetramethylrhodamine (TRITC) for fluorescence detection) at 37 °C for 24 and 48 h. The HeLa cells nuclei were stained with DAPI, and the cytoskeletons of the cells were stained with Alexa Fluor 488 by the standard procedure. Fluorescence micrographs of HeLa cells with the internalized particles were recorded with a confocal microscope (Leica TCS SP5 X). Divided and not fully depicted cells were not considered for analysis. Imaging was performed by taking into account the staining of the action network which delineated the cell shape (green fluorescence coming from fluorescently labeled Alexa Fluor), the nucleus inside each cell (blue fluorescence coming from DAPI), and microcontainers (in red fluorescently labeled). Microcontainers adherent to the outer cell plasma membrane and in between the grown cells were clearly distinguished from the microcapsules which were located inside of cells, located separately from the cytoskeleton. Based on these confocal images, histograms showed the number of internalized particles per cell $f(N)$, and the corresponding cumulative distribution functions (CDFs) $p(N)$ were generated (Figure 11). Standard deviations were calculated from the deviation of the independent $f(N)$ or CDFs of two different experiments per each data set. The histogram $f(N)$ describes the frequency f, i.e., the number of events, in which cells with exactly N internalized microcapsules were observed. The CDF $p(N)$ indicates the probability that a cell contains N or less microcapsules internalized. For example, $p(N = 3)$ is the probability to find cells with either 0, 1, 2, or 3 internalized microcapsules. CDFs are directly calculated from histograms where $p(N)$:

$$p(N) = \sum_{(i=0)}^{N} f(i) / \sum_{(i=0)}^{\infty} f(i) \quad (2)$$

These values are used to make the differences of microcontainer uptake easier to be visualized. The CDFs are normalized and thus $0 \leq p(N) \leq 1$.

RESULTS AND DISCUSSION

To study the influence of the calcium carbonate template on silver alginate microcapsules via the method described in our previous work[45] and presented in Figure 1, calcium carbonate templates with different sizes were used. These templates were synthesized by three different methods: assisted by magnetic stirring,[49] by ultrasonically stirring the mixture,[47] and synthesis in ethylene glycol solution[50] with the sizes 3.0 ± 0.3, 1.0 ± 0.2, and 0.8 ± 0.1 μm correspondingly (Figure 2a–c).

Hydrogel microcapsules were obtained by alginate adsorption on the porous spherical calcium carbonate microparticles, followed by hydrogel cross-linking by silver ions after adding silver nitrate. Reduction of silver nanoparticles on the alginate matrix and simultaneous removal of calcium carbonate cores was achieved by the addition of ascorbic acid solution. The size of the resulting microcapsules is completely determined by the size of the calcium carbonate template and is equal to 3.0 ± 0.8, 2.0 ± 0.2, and 0.9 ± 0.1 μm of calcium carbonate cores respectively (Figure 2d–f).

The STEM images (Figure 3a) demonstrated that the shells of the silver alginate microcapsules were formatted from the reduction of the silver ions and contained few layers of the silver nanoparticles. The average size of these nanoparticles is 35 ± 9 nm (Figure 3g). We found a high density of twins (Figure 3d–f) in the nanoparticles, which are a typical defect in silver nanoparticles.[51]

Alginate microcapsules were loaded with protein labeled TRITC–BSA in order to demonstrate functionality of the microcontainers as drug delivery carriers. The confocal scanning laser microscopy image reveals that TRITC–BSA was successfully embedded in the structure of alginate microcontainers (Figure 4a–c).

The loading capacities of the silver alginate microcontainers have been estimated by spectrophotometry which revealed that more (or comparable amount) of the functional substance can be loaded to large alginate capsules. Such loading capacity is relatively high with respect to the initial $CaCO_3$ particles (5%) because during the alginate synthesis we eliminate the heaviest part of the capsules: the calcium carbonate core (80% of the total particle weight).

Ultrasound Release. To demonstrate the payload release activated by the ultrasound treatment, the water suspension of the microcontainers was placed under US treatment for different time intervals up to 180 min. Two parameters were investigated: (1) percentage of released TRITC–BSA molecules in supernatant (Figure 4) and (2) percentage of crashed microcontainers (Figure 5). To confirm the much more strong effect of ultrasonic treatment on the release process, the US treated microcontainers were compared with nonultrasonically treated microcontainers: control (size 3.0 ± 0.8 μm; Figure 5). All control microcapsules

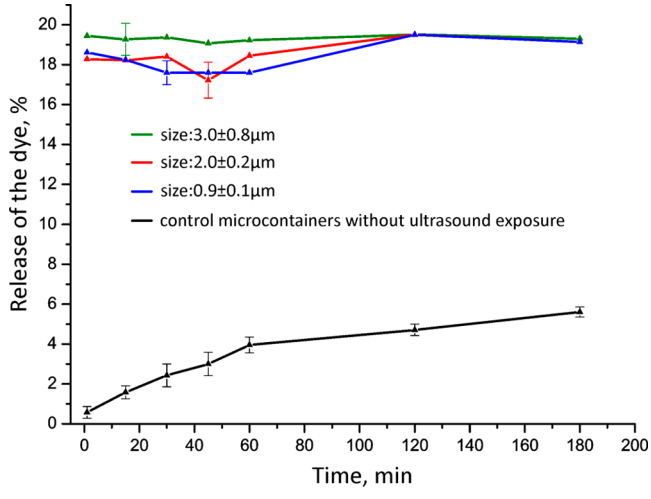

Figure 5. Release of the TRITC–BSA dependence on the time of US exposure.

DOI: 10.1021/acsami.7b08147
ACS Appl. Mater. Interfaces 2017, 9, 21949–21958

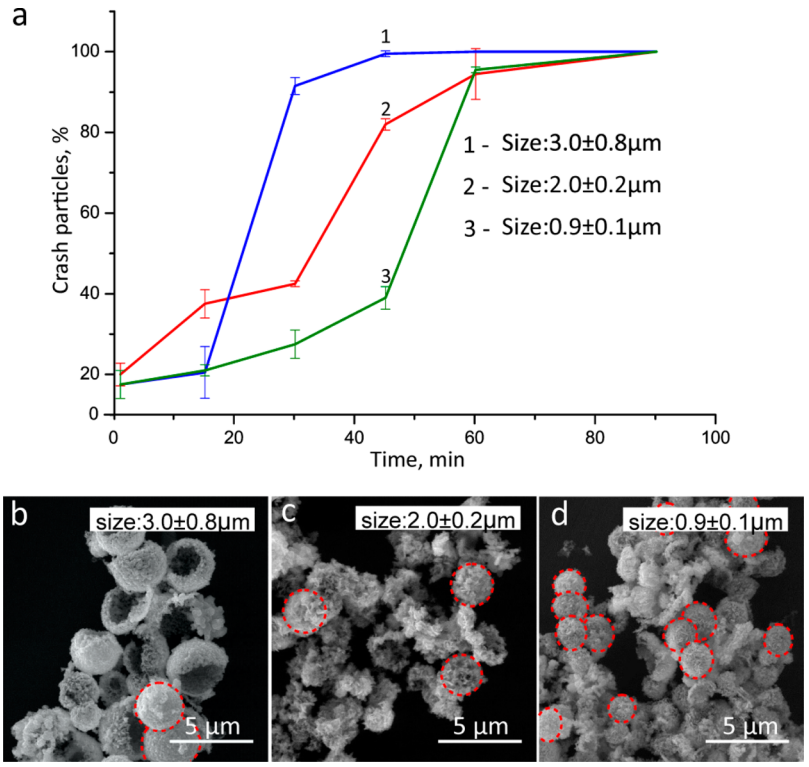

Figure 6. (a) Number of crashed microcontainers dependence on the time of ultrasound treatment (frequency 35 kHz and power density 0.64 W/cm^2) for the silver alginate microcontainers with different sized curves (1) 3.0 ± 0.8, (2) 2.0 ± 0.2, and (3) 0.9 ± 0.1 μm (Supporting Information, Table S1). (b–d) SEM images of the hollow silver alginate microcapsules of different sizes: (b) 3.0 ± 0.8, (c) 2.0 ± 0.2, and (d) 0.9 ± 0.1 μm after the ultrasound treatment (frequency 35 kHz and power density 0.64 W/cm^2). The duration of US treatment is 60 min. Images correspond to spherical silver alginate hydrogel microcontainers indicated with red dashed circles.

were stable during the 3 h of immersion in water, and release was not more than 6% of encapsulated TRITC–BSA. A tTypical release profile is presented in Figure 5 (black curve). Such a dynamic corresponds to the spontaneous diffusion of the payload molecules. In contrast for US treatment, the release was stimulated by the microcontainers crashing as well as the enhancement of molecule diffusion speed by the US. In this case more than 18% of encapsulated TRITC–BSA molecules were released in 1 min which corresponds to 20% of crashed microcontainers. In later time crashed the microcontainer amount increased and reached 99% after 3 h of treatment. However, the amount of the released molecules does not increase as dramatically. It can happen because the experiment occurs in close to 1 mL volume, and the released protein can adsorb back into pieces of the silver alginate microcontainers.

After 100 min of US treatment, all particles have been collapsed independently on the microcontainers size (Figure 6). This corresponds with the maximum amount of release from all samples. Short exposition times (less than 10 min) do not lead to a significant increase of the number of crashed microcontainers (only for 0.9 μm-sized microcontainers, the number of crashed microcontainers increased from 17 to 38). It is possible to attain the destruction of 80% microcontainers at time intervals, which depend on the microcontainers size (Figure 6b–d). However, after 30 min of ultrasonic treatment, samples with the largest diameter were completely destroyed (Figure 6a).

The density of 3.0 ± 0.8 μm microcontainers is higher than these microcontainers which appeared to be more firm. However, due to ascorbic acid treatment, a particle's shell has an inhomogeneity of density, which lead to the breaking of the thinnest area and rapid destruction of the capsule during US treatment (Figure 6b).

Microcontainers densities of sizes 2.0 ± 0.2 and 0.9 ± 0.1 μm are almost commensurable; however, our intention is that in microcontainers of size 2.0 ± 0.2 μm, the affect is the same as that in microcontainers of size 3.0 ± 0.8 μm.

Scanning electron microscopy images (Figure 6d) show that silver alginate microcontainers with size 0.9 ± 0.1 μm are stable under the ultrasound influence, since it has a uniform coating. Payload molecules are placed generally in silver alginate matrix. Due to this fact, microcapsules do not have a significant release rate and can adsorb back on the surface of crashed capsules.

Raman Investigations. We determine the SERS (SSEF) substrate enhancement factor[48] by labeling the microcontainers with 4-nitrothiophenol. Average SERS spectra of this molecule on the microcontainers are shown in Figure 7. The SSEF is calculated

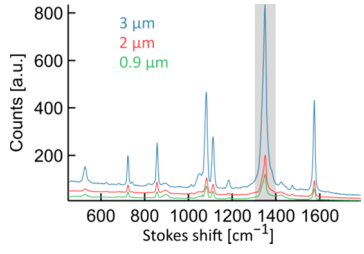

Figure 7. NTP SERS spectra for the different sizes of microcontainers. The 1339 cm^1 peak, which is used for calculating the enhancement factor, is highlighted in gray. Each spectrum is an average over different clusters of microcontainers.

DOI: 10.1021/acsami.7b08147
ACS Appl. Mater. Interfaces 2017, 9, 21949–21958

from the Stokes scattering intensity per molecule in a SERS experiment versus a conventional bulk Raman measurement on the same molecule:

$$\mathrm{SSEF} = \frac{I_{\mathrm{SERS}} P_{\mathrm{Raman}}}{I_{\mathrm{Raman}} P_{\mathrm{SERS}}} \frac{N_{\mathrm{Raman}}}{N_{\mathrm{SERS}}} = \frac{I_{\mathrm{SERS}} P_{\mathrm{Raman}}}{I_{\mathrm{Raman}} P_{\mathrm{SERS}}} \frac{H_{\mathrm{eff}}}{\rho \mu_{\mathrm{Ag}}} \quad (3)$$

Here the intensities are rescaled for differences in Raman pump power (P_{Raman} and P_{SERS}). A reference spectrum of a bulk solution of molecules is measured in a confocal volume with an effective height H_{eff} of 160 μm and a concentration c of 3×10^{25} particles/m^3. The number of molecules contributing to the SERS signal is determined by a surface density of the molecules ρ of approximately 4.4×10^{18} particles/m^2[52] and a projected area fraction μ_{Ag} of the silver surface of 2.8 (according to the TEM microscope images).

SERS data is analyzed based on the 1339 cm^{-1} peak (symmetric stretching mode of NO_2). We find an enhancement factor in the range of 10^4–10^5 for all types of microcontainers (Figure 8),

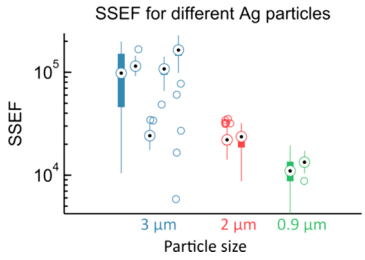

Figure 8. SSEF calculated on the different microcontainers showing a value of 10^4–10^5. Each bar represents multiple points measured on a separate cluster of microcontainers.

which nicely correlates with the literature data.[53] The rather large variation in enhancement factors can be explained by the inhomogeneous, self-assembled clusters of microcontainers on which the SERS spectra are acquired. For each different set of particles, Raman spectra were acquired in at least two maps of 40 × 40 μm with 10 × 10 pixels.

The largest microcontainers demonstrate the better amplification properties as well as highest variation of enhancement coefficient. It possible to explain that more uniform distribution of the silver nanoparticles in the largest alginate shells provides a better distance among the silver nanoparticles. However, increasing of amount of the areas of inhomogeneity, which is typical for largest particles, leads to increasing the dispersion of the SERS signal.

Therefore, using these silver monovalent ions for cross-linked alginate chain allow us to obtain a less stable shell than the in the case of bivalent ions like Ca^{2+}, Mg^{2+}, Co^{2+}, Cu^{2+}, and Cd^{2+}. Using silver ions as structural elements for silver nanoparticles, which was obtained via in situ synthesis on alginate bead surface, allows us to obtain beads with homogeneous distribution of silver nanoparticles in their shells as well as to reach the optimal distance between silver nanoparticles, which allows us to increase the Raman signal up to 10^5.

Cellular Cytotoxicity and Uptake. For the study the cell toxicity, the different concentration microcontainers from 10 particles/cell to 100 particles/cell were incubated with HeLa cells. As a first step, the particles were dispersed in PBS buffer and added to the cell culture.

As a control experiment, the microcontainers were incubated in PBS buffer for 24 h (37 °C), and the morphology and drug release have been studied. The SEM images (Supporting Information, Figure S2) demonstrated that there is no significant difference in morphology, and the release profiles were similar to the water incubation as is present in Figure 5.

The cells with capsules after 24 and 48 h of culturing had a well-spread morphology typical of attached cells, with the morphology typical for spreading HeLa cells line; they are attached with their pseudopodia to plastic and exhibit sufficient cell adhesion. The quantity assay related to percent of surviving cells is presented in Figure 9.

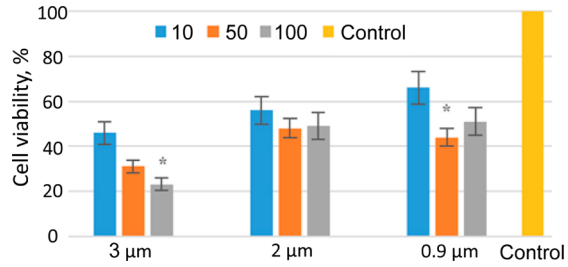

Figure 9. Results of cytotoxicity tests of silver alginate hydrogel microcontainers on cell line HeLa. An asterisk (*) indicates significant differences from the data for the same particle's sizes.

The lowest toxicity demonstrates the of silver alginate hydrogel microcontainers for 10 particles/cell concentration. Increasing the amount of the microcontainers lead to an increase in the toxicity until 50% of the control cells. The highest toxicity effect demonstrates the particles with largest particles. It is possible to be explained by the large surface area of one particles and the large amount of the free silver ions.[54] Smaller particles have a more dense structure as described above and as a result decrease the diffusion rate of the free silver ions.

Since the metabolic activity was higher (less toxicity) for a lower particle/cell ratio, a standard concentration of 10 microcontainers/cell was selected during all subsequent experiments. The number of internalized particles per cell was evaluated after 24 and 48 h of incubation by counting the particles inside HeLa cells via fluorescence microscopy and subsequent image analysis. The cell cytoskeleton and nucleus were fluorescently stained, and the colocalization of the red fluorescently labeled microcontainers with in the cellular compartments was evaluated with z-stack images as shown in Figure 10.

To estimate the efficiency of the penetration silver alginate microcontainers though the cell membrane, the cumulative probability of the presenting microcapsules inside the cell was estimated by confocal microscopy, and the results are presented in Figure 11, CDFs of 3, 2, and 0.9 μm microcontainers. After 24 h with silver alginate hydrogel microcontainers, 3 μm and 2 μm capsules were taken up by the cells to a similar extent. The 0.9 μm microcapsules were internalized to a much higher extent than all other microcontainers, pointing at a correlation between the size of microcontainers and their uptake. For example 80% of cells in 24 h have not more than 7 particles with sizes 2 or 3 μm in comparison with 80% of cells have not more than 11 particles with size 0.9 μm. Thus, their differences after 48 h due to cell fission shows that the microcontainer's distribution becomes much more even (Figure 11b).

Thus, all sizes of alginate microcontainers can penetrate through the cell membrane, and it is possible that it can be used as a drug delivery system.

DOI: 10.1021/acsami.7b08147
ACS Appl. Mater. Interfaces 2017, 9, 21949–21958

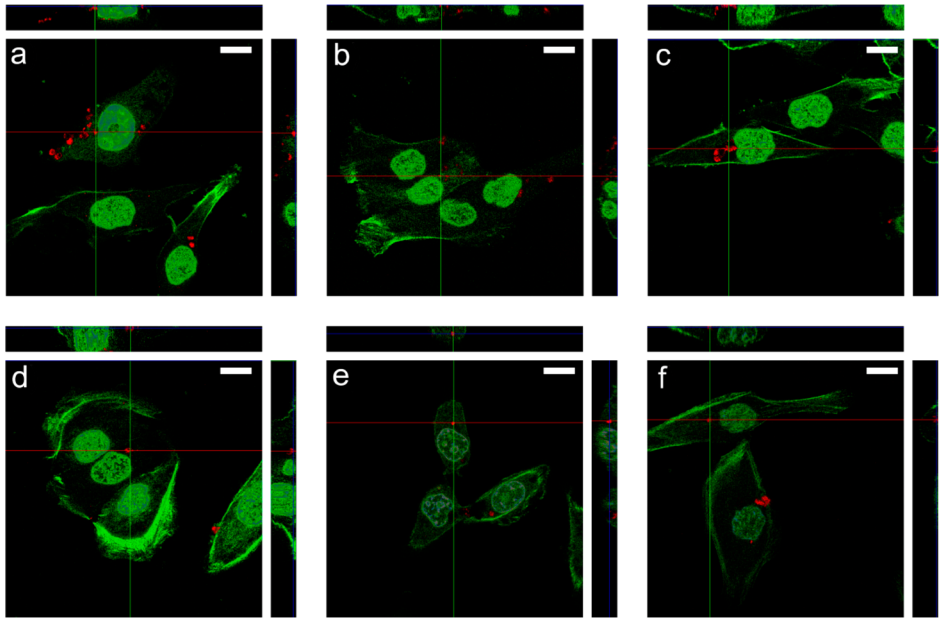

Figure 10. Orthogonal view from different planes (x/y, x/z, or y/z) of the confocal microscope images of HeLa cells which internalized differently shaped microcontainers after incubation for 24 and 48 h. (a) 3 μm microcontainers after 24 h, (b) 2 μm microcontainers after 24 h, (c) 0.9 μm microcontainers after 24 h, (d) 3 μm microcontainers after 48 h, (e) 2 μm microcontainers after 48 h, and (f) 0,9 μm microcontainers after 48 h. Colocalization of fluorescently labeled silver alginate hydrogel microcontainers (with TRITC, in red). The HeLa cells nuclei were stained with DAPI (in blue) and the cytoskeletons with Alexa Fluor 488 (in green). Scale bars correspond to 15 μm.

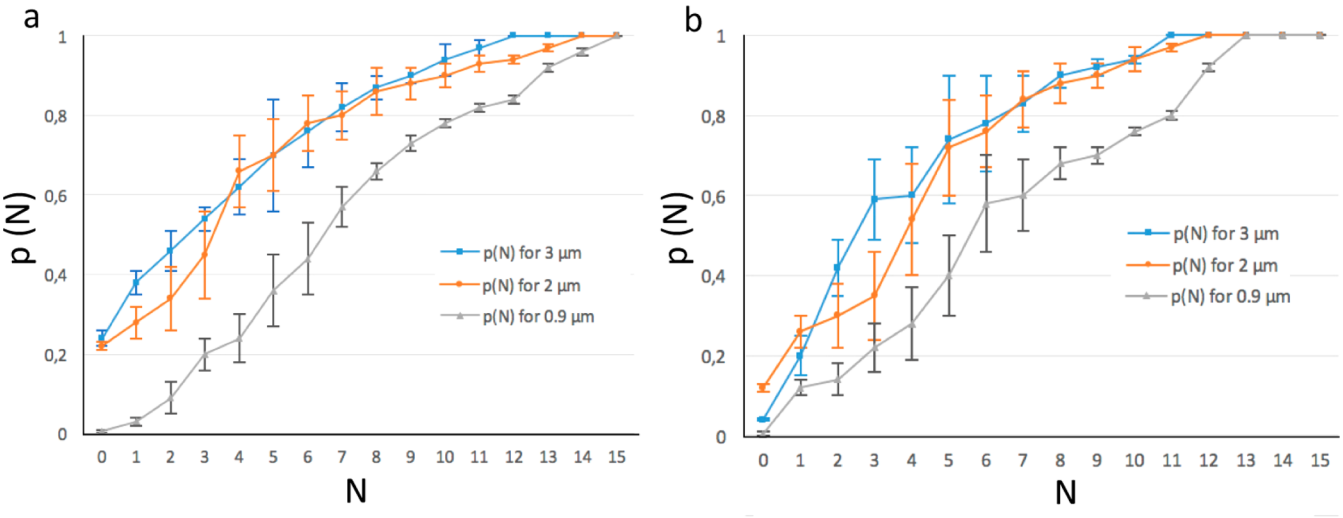

Figure 11. Cumulative probability $p(N)$ for N internalized microcontainers per cell for microcontainers with different sizes after (a) 24 and (b) 48 h of microcontainers incubation with a concentration of 10 added capsules per cell. 3 (blue dots), 2 (orange dots), and 0.9 μm (gray dots). The vertical bars represent the standard deviation values.

CONCLUSIONS

In this study, we have demonstrated a simple way of fabricating biocompatible hollow microcapsules of various sizes based on calcium carbonate templates, alginate matrix, and silver nanoparticles. Silver alginate hydrogel microcapsules serve as microcontainers with a functional substance payload. Loading efficacy depends on the microcapsules size, which can be varied from 0.9 ± 0.1 μm for the smallest particles up to 3.0 ± 0.8 μm for the largest microcontainers. Release of encapsulated materials by ultrasound was realized using intensities allowed in medicine. It was found that larger particle shells (3.0 ± 0.8 μm) are less effective for ultrasound release, while the highest efficiency of release was realized for small microcontainers (0.9 ± 0.1 μm).

In addition, silver alginate microcontainers demonstrate the possibility to enhance the Raman signal of up to 10^5 fold: a magnitude which is in the range for applications in theranostics.[55] Analysis of the structure of silver nanoparticles, which are important for both SERS and enhancement of mechanical properties, was performed using high resolution electron microscopy; interestingly, twin structures were discovered.

The developed microcontainers are attractive for applications in biomedicine and cell biology. Cell experiments (with HeLa cells) have shown the low toxicity of silver alginate hydrogel microcontainers for small concentrations and an increase in toxicity for strong concentrations, using qualitative (proliferation, adhesion, and morphology of cell line) and quantitative (MTT)

DOI: 10.1021/acsami.7b08147
ACS Appl. Mater. Interfaces 2017, 9, 21949−21958

methods. Also, an effective uptake by cells has been observed studying the cumulative probability of the uptake, the probability of the uptake of no more than a certain number of microcontainers. A number was found up to 15 particles per cell at 24 h and up to 13 particles per cell at 48 h, taking into account the influence of the cell division. Smaller particles are uptaken by cells more effectively than bigger ones.

An easy fabrication process as well as green chemistry components[56−59] make the alginate hydrogel particles a potentially attractive drug delivery carrier. Double functionality (drug delivery and detection) of the silver alginate containers represents an attractive candidate of theranostic concept for personalized medicine.

■ ASSOCIATED CONTENT

Supporting Information

The Supporting Information is available free of charge on the ACS Publications website at DOI: 10.1021/acsami.7b08147.

Table representing the number of crashed particles and its dependence on the time of ultrasound treatment, controlled the spontaneous SERS spectra. (PDF)

■ AUTHOR INFORMATION

Corresponding Author

*E-mail: LengertKatrin@mail.ru; Ekaterina.Lengert@UGent.be.

ORCID

Ekaterina Lengert: 0000-0002-6447-2811

Pieter C. Wuytens: 0000-0002-0793-256X

Author Contributions

The manuscript was written through contributions of all authors. All authors have given approval to the final version of the manuscript.

Notes

The authors declare no competing financial interest.

■ ACKNOWLEDGMENTS

We would like to thank N. N. Efimova and V. F. Lengert for fruitful discussion and support. The study was supported by the Government of the Russian Federation (Grant No. 14. Z50.31.0004 to support scientific research projects implemented under the supervision of leading scientists at Russian institutions and Russian institutions of higher education) and Russian Foundation for Basic Research (RFBR research Project No. 15-29-01172 ofi_m). A.G.S. acknowledges FWO (Vlaanderen) and BOF UGent for support. The ERA-Net Rus Plus program is acknowledged for support in the framework of the project "Fabrication and investigation of new hybrid scaffolds with the controlled porous hierarchy for bone tissue engineering" (Intelbiocomp). E.L. acknowledges scholarships of the President of the Russian Federation on training abroad in the 2016/2017 academic year. B.P. thanks the Research Foundation Flanders (FWO) for postdoctoral research fellowships.

■ REFERENCES

(1) Vergaro, V.; Scarlino, F.; Bellomo, C.; Rinaldi, R.; Vergara, D.; Maffia, M.; Baldassarre, F.; Giannelli, G.; Zhang, X.; Lvov, Y. M.; Leporatti, S. Drug-Loaded Polyelectrolyte Microcapsules for Sustained Targeting of Cancer Cells. *Adv. Drug Delivery Rev.* **2011**, *63*, 847−864.

(2) Parakhonskiy, B. V.; Yashchenok, A. M.; Konrad, M.; Skirtach, A. G. Colloidal Micro- and Nano-Particles as Templates for Polyelectrolyte Multilayer Capsules. *Adv. Colloid Interface Sci.* **2014**, *207* (1), 253−264.

(3) Skirtach, A. G.; Yashchenok, A. M.; Möhwald, H. Encapsulation, Release and Applications of LbL Polyelectrolyte Multilayer Capsules. *Chem. Commun.* **2011**, *47* (48), 12736.

(4) Wuytens, P.; Parakhonskiy, B.; Yashchenok, A.; Winterhalter, M.; Skirtach, A. Pharmacological Aspects of Release from Microcapsules - From Polymeric Multilayers to Lipid Membranes. *Curr. Opin. Pharmacol.* **2014**, *18*, 129−140.

(5) Reguera, J.; Jiménez de Aberasturi, D.; Winckelmans, N.; Langer, J.; Bals, S.; Liz-Marzán, L. M. Synthesis of Janus Plasmonic−magnetic, Star−sphere Nanoparticles, and Their Application in SERS Detection. *Faraday Discuss.* **2016**, *191*, 47−59.

(6) Fales, A. M.; Yuan, H.; Vo-Dinh, T. Silica-Coated Gold Nanostars for Combined Surface-Enhanced Raman Scattering (SERS) Detection and Singlet-Oxygen Generation: A Potential Nanoplatform for Theranostics. *Langmuir* **2011**, *27* (19), 12186−12190.

(7) Evanoff, D. D.; Chumanov, G. Synthesis and Optical Properties of Silver Nanoparticles and Arrays. *ChemPhysChem* **2005**, *6*, 1221−1231.

(8) Lu, C. H.; Willner, I. Stimuli-Responsive DNA-Functionalized Nano-/Microcontainers for Switchable and Controlled Release. *Angew. Chem., Int. Ed.* **2015**, *54* (42), 12212−12235.

(9) Parakhonskiy, B. V.; Bedard, M.; Bukreeva, T.; Sukhorukov, G. B.; Möhwald, H.; Skirtach, A. G. Nanoparticles on Polyelectrolytes at Low Concentration: Controlling Concentration and Size. *J. Phys. Chem. C* **2010**, *114* (5), 1996−2002.

(10) Abalde-Cela, S.; Aldeanueva-Potel, P.; Mateo-Mateo, C.; Rodríguez-Lorenzo, L.; Alvarez-Puebla, R. A.; Liz-Marzán, L. M. Surface-Enhanced Raman Scattering Biomedical Applications of Plasmonic Colloidal Particles. *J. R. Soc., Interface* **2010**, *7*, S435−S450.

(11) Saha, S.; Pal, A.; Pande, S.; Sarkar, S.; Panigrahi, S.; Pal, T. Alginate Gel-Mediated Photochemical Growth of Mono- and Bimetallic Gold and Silver Nanoclusters and Their Application to Surface-Enhanced Raman Scattering. *J. Phys. Chem. C* **2009**, *113*, 7553−7560.

(12) Prikhozhdenko, E. S.; Lengert, E. V.; Parakhonskiy, B. V.; Gorin, D. A.; Sukhorukov, G. B.; Yashchenok, A. M. Biocompatible Chitosan Nanofibers Functionalized with Silver Nanoparticles for SERS Based Detection. *Acta Phys. Pol., A* **2016**, *129* (2), 247−249.

(13) Bédard, M. F.; Munoz-Javier, A.; Mueller, R.; del Pino, P.; Fery, A.; Parak, W. J.; Skirtach, A. G.; Sukhorukov, G. B. On the Mechanical Stability of Polymeric Microcontainers Functionalized with Nanoparticles. *Soft Matter* **2009**, *5* (1), 148.

(14) Skirtach, A. G.; De Geest, B. G.; Mamedov, A.; Antipov, A. A.; Kotov, A.; Sukhorukov, G. B. Ultrasound Stimulated Release and Catalysis Using Polyelectrolyte Multilayer Capsules. *J. Mater. Chem.* **2007**, *17*, 1050−1054.

(15) Maneerung, T.; Tokura, S.; Rujiravanit, R. Impregnation of Silver Nanoparticles into Bacterial Cellulose for Antimicrobial Wound Dressing. *Carbohydr. Polym.* **2008**, *72* (1), 43−51.

(16) Wang, A.; Cui, Y.; Yang, Y.; Li, J. Capsules with Silver Nanoparticle Enrichment Subdomains and Their Antimicrobial Properties. *Chem. - Asian J.* **2010**, *5* (8), 1780−1787.

(17) Kim, J. S.; Kuk, E.; Yu, K. N.; Kim, J.-H.; Park, S. J.; Lee, H. J.; Kim, S. H.; Park, Y. K.; Park, Y. H.; Hwang, C.-Y.; Kim, Y.-K.; Lee, Y.-S.; Jeong, D. H.; Cho, M.-H. Antimicrobial Effects of Silver Nanoparticles. *Nanomedicine* **2007**, *3* (1), 95−101.

(18) Prabhu, S.; Poulose, E. K. Silver Nanoparticles: Mechanism of Antimicrobial Action, Synthesis, Medical Applications, and Toxicity Effects. *Int. Nano Lett.* **2012**, *2* (1), 32.

(19) Wei, D.; Sun, W.; Qian, W.; Ye, Y.; Ma, X. The Synthesis of Chitosan-Based Silver Nanoparticles and Their Antibacterial Activity. *Carbohydr. Res.* **2009**, *344* (17), 2375−2382.

(20) Koga, H.; Kitaoka, T. On-Paper Synthesis of Silver Nanoparticles for Antibacterial Applications. *Silver Nanoparticles* **2008**, 277−295.

(21) Yang, J.; Zheng, H.; Han, S.; Jiang, Z.; Chen, X. The Synthesis of Nano-Silver/sodium Alginate Composites and Their Antibacterial Properties. *RSC Adv.* **2015**, *5*, 2378−2382.

(22) Yashchenok, A. M.; Delcea, M.; Videnova, K.; Jares-Erijman, E. A.; Jovin, T. M.; Konrad, M.; Möhwald, H.; Skirtach, A. G. Enzyme Reaction in the Pores of CaCO3 Particles upon Ultrasound Disruption of Attached

DOI: 10.1021/acsami.7b08147
ACS Appl. Mater. Interfaces 2017, 9, 21949−21958

Substrate-Filled Liposomes. *Angew. Chem., Int. Ed.* **2010**, *49* (44), 8116−8120.
(23) del Mercato, L. L.; Rivera Gil, P.; Abbasi, A. Z.; Ochs, M.; Ganas, C.; Zins, I.; Sönnichsen, C.; Parak, W. J. LbL Multilayer Capsules: Recent Progress and Future Outlook for Their Use in Life Sciences. *Nanoscale* **2010**, *2* (4), 458−467.
(24) Itoh, Y.; Matsusaki, M.; Kida, T.; Akashi, M. Enzyme-Responsive Release of Encapsulated Proteins from Biodegradable Hollow Capsules. *Biomacromolecules* **2006**, *7* (10), 2715−2718.
(25) Sukhorukov, G. B.; Antipov, A. A.; Voigt, A.; Donath, E.; Mohwald, H. pH-Controlled Macromolecule Encapsulation in and Release from Polyelectrolyte Multilayer Nanocapsules. *Macromol. Rapid Commun.* **2001**, *22* (1), 44−46.
(26) Rosenbauer, E. M.; Wagner, M.; Musyanovych, A.; Landfester, K. Controlled Release from Polyurethane Nanocapsules via pH-, UV-Light- or Temperature-Induced Stimuli. *Macromolecules* **2010**, *43* (11), 5083−5093.
(27) Kozlovskaya, V.; Kharlampieva, E.; Mansfield, M. L.; Sukhishvili, S. A. Poly(methacrylie Acid) Hydrogel Films and Capsules: Response to pH and Ionic Strength, and Encapsulation of Macromolecules. *Chem. Mater.* **2006**, *18* (2), 328−336.
(28) Elsner, N.; Kozlovskaya, V.; Sukhishvili, S. A.; Fery, A. pH-Triggered Softening of Crosslinked Hydrogen-Bonded Capsules. *Soft Matter* **2006**, *2* (11), 966−972.
(29) Parakhonskiy, B. V.; Foss, C.; Carletti, E.; Fedel, M.; Haase, A.; Motta, A.; Migliaresi, C.; Antolini, R. Tailored Intracellular Delivery via a Crystal Phase Transition in 400 Nm Vaterite Particles. *Biomater. Sci.* **2013**, *1* (12), 1273.
(30) Parakhonskiy, B. V.; Haase, A.; Antolini, R. Sub-Micrometer Vaterite Containers: Synthesis, Substance Loading, and Release. *Angew. Chem., Int. Ed.* **2012**, *51* (5), 1195−1197.
(31) Shchukin, D. G.; Gorin, D. A.; Möhwald, H. Ultrasonically Induced Opening of Polyelectrolyte Microcontainers. *Langmuir* **2006**, *22* (17), 7400−7404.
(32) Kolesnikova, T. A.; Gorin, D. A.; Fernandes, P.; Kessel, S.; Khomutov, G. B.; Fery, A.; Shchukin, D. G.; Möhwald, H. Nanocomposite Microcontainers with High Ultrasound Sensitivity. *Adv. Funct. Mater.* **2010**, *20* (7), 1189−1195.
(33) Anandhakumar, S.; Mahalakshmi, V.; Raichur, A. M. Silver Nanoparticles Modified Nanocapsules for Ultrasonically Activated Drug Delivery. *Mater. Sci. Eng., C* **2012**, *32* (8), 2349−2355.
(34) Long, Y.; Liu, C. Y.; Zhao, B.; Song, K.; Yang, G. Q.; Tung, C. H. Bio-Inspired Controlled Release through Compression-Relaxation Cycles of Microcapsules. *NPG Asia Mater.* **2015**, *7* (1), e148.
(35) Chang, M.-W.; Edirisinghe, M.; Stride, E. Ultrasound Mediated Release from Stimuli-Responsive Core-Shell Capsules. *J. Mater. Chem. B* **2013**, *1* (32), 3962−3971.
(36) Ariga, K.; Lvov, Y. M.; Kawakami, K.; Ji, Q.; Hill, J. P. Layer-by-Layer Self-Assembled Shells for Drug Delivery. *Adv. Drug Delivery Rev.* **2011**, *63* (9), 762−771.
(37) Korolovych, V. F.; Grishina, O. A.; Inozemtseva, O. A.; Selifonov, A. V.; Bratashov, D. N.; Suchkov, S. G.; Bulavin, L. A.; Glukhova, O. E.; Sukhorukov, G. B.; Gorin, D. A. Impact of High-Frequency Ultrasound on Nanocomposite Microcapsules: In Silico and in Situ Visualization. *Phys. Chem. Chem. Phys.* **2016**, *18* (4), 2389−2397.
(38) Sboros, V. Response of Contrast Agents to Ultrasound. *Adv. Drug Delivery Rev.* **2008**, *60*, 1117−1136.
(39) Lin, H. Y.; Thomas, J. L. Factors Affecting Responsivity of Unilamellar Liposomes to 20 kHz Ultrasound. *Langmuir* **2004**, *20* (15), 6100−6106.
(40) Pavlov, A. M.; Saez, V.; Cobley, A.; Graves, J.; Sukhorukov, G. B.; Mason, T. J. Controlled Protein Release from Microcapsules with Composite Shells Using High Frequency Ultrasound—potential for in Vivo Medical Use. *Soft Matter* **2011**, *7* (9), 4341.
(41) Albanese, A.; Tang, P. S.; Chan, W. C. W. [Review] The Effect of Nanoparticle Size, Shape, and Surface Chemistry on Biological Systems. *Annu. Rev. Biomed. Eng.* **2012**, *14* (1), 1−16.
(42) Parakhonskiy, B.; Zyuzin, M. V.; Yashchenok, A.; Carregal-Romero, S.; Rejman, J.; Möhwald, H.; Parak, W. J.; Skirtach, A. G. The Influence of the Size and Aspect Ratio of Anisotropic, Porous CaCO3 Particles on Their Uptake by Cells. *J. Nanobiotechnol.* **2015**, *13* (1), 53.
(43) Chen, J.; Ratnayaka, S.; Alford, A.; Kozlovskaya, V.; Liu, F.; Xue, B.; Hoyt, K.; Kharlampieva, E. Theranostic Multilayer Capsules for Ultrasound Imaging and Guided Drug Delivery. *ACS Nano* **2017**, *11* (3), 3135−3146.
(44) Xiong, R.; Soenen, S. J.; Braeckmans, K.; Skirtach, A. G. Towards Theranostic Multicompartment Microcapsules: In-Situ Diagnostics and Laser-Induced Treatment. *Theranostics* **2013**, *3* (3), 141−151.
(45) Lengert, E.; Yashchenok, A. M.; Atkin, V.; Lapanje, A.; Gorin, D. A.; Sukhorukov, G. B.; Parakhonskiy, B. V. Hollow Silver Alginate Microspheres for Drug Delivery and Surface Enhanced Raman Scattering Detection. *RSC Adv.* **2016**, *6* (24), 20447−20452.
(46) Volodkin, D. V.; Petrov, A. I.; Prevot, M.; Sukhorukov, G. B. Matrix Polyelectrolyte Microcapsules: New System for Macromolecule Encapsulation. *Langmuir* **2004**, *20* (8), 3398−3406.
(47) Svenskaya, Y. I.; Fattah, H.; Zakharevich, A. M.; Gorin, D. A.; Sukhorukov, G. B.; Parakhonskiy, B. V. Ultrasonically Assisted Fabrication of Vaterite Submicron-Sized Carriers. *Adv. Powder Technol.* **2016**, *27* (2), 618−624.
(48) Le Ru, E. C.; Etchegoin, P. G. Quantifying SERS Enhancements. *MRS Bull.* **2013**, *38* (8), 631−640.
(49) Volodkin, D. V.; von Klitzing, R.; Möhwald, H. Pure Protein Microspheres by Calcium Carbonate Templating. *Angew. Chem., Int. Ed.* **2010**, *49* (48), 9258−9261.
(50) Ryu, M.; Ahn, J.; You, K.; Goto, S.; Kim, H. Synthesis of Calcium Carbonate in Ethanol-Ethylene Glycol Solvent. *J. Ceram. Soc. Jpn.* **2009**, *117*, 106−110.
(51) Zhang, X. B.; Vasiliev, A. L.; Van Tendeloo, G.; He, Y.; Yu, L. M.; Thiry, P. A. EM, XPS and LEED Study of Deposition of Ag on Hydrogenated Si Substrate Prepared by Wet Chemical Treatments. *Surf. Sci.* **1995**, *340* (3), 317−327.
(52) Baia, L.; Baia, M.; Popp, J.; Astilean, S. Gold Films Deposited over Regular Arrays of Polystyrene Nanospheres as Highly Effective SERS Substrates from Visible to NIR. *J. Phys. Chem. B* **2006**, *110* (47), 23982−23986.
(53) Prikhozhdenko, E. S.; Atkin, V. S.; Parakhonskiy, B. V.; Rybkin, I. A.; Lapanje, A.; Sukhorukov, G. B.; Gorin, D. A.; Yashchenok, A. M. New Post-Processing Method of Preparing Nanofibrous SERS Substrates with a High Density of Silver Nanoparticles. *RSC Adv.* **2016**, *6* (87), 84505−84511.
(54) Navarro, E.; Piccapietra, F.; Wagner, B.; Marconi, F.; Kaegi, R.; Odzak, N.; Sigg, L.; Behra, R. Toxicity of Silver Nanoparticles to Chlamydomonas Reinhardtii. *Environ. Sci. Technol.* **2008**, *42* (23), 8959−8964.
(55) Prikhozhdenko, E. S.; Atkin, V. S.; Parakhonskiy, B. V.; Rybkin, I. A.; Lapanje, A.; Sukhorukov, G. B.; Gorin, D. A.; Yashchenok, A. M. New Post-Processing Method of Preparing Nanofibrous SERS Substrates with a High Density of Silver Nanoparticles. *RSC Adv.* **2016**, *6* (87), 84505−84511.
(56) Vallejo, R.; Segovia, P.; Elizondo, N.; Vázquez, O.; Coello, V.; Castaño, V. Green Chemistry Used in the Synthesis and Characterization of Silver and Gold Nanoparticles. *Nanotechnol. 2010 Adv. Mater. CNTs, Part. Film. Compos. - Technol. Proc. 2010 NSTI Nanotechnol. Conf. Expo, NSTI-Nanotech 2010* **2010**, *1*, 482−484.
(57) Otari, S. V.; Patel, S. K. S.; Jeong, J.-H.; Lee, J. H.; Lee, J.-K. A Green Chemistry Approach for Synthesizing Thermostable Antimicrobial Peptide-Coated Gold Nanoparticles Immobilized in an Alginate Biohydrogel. *RSC Adv.* **2016**, *6* (90), 86808−86816.
(58) Yao, C.; Xie, A.; Shen, Y.; Zhu, J.; Li, T. Green Synthesis of Calcium Carbonate with Unusual Morphologies in the Presence of Fruit Extracts. *J. Chil. Chem. Soc.* **2013**, *58* (4), 2235−2238.
(59) Hwang, E. T.; Gang, H.; Chung, J.; Gu, M. B. Carbonic Anhydrase Assisted Calcium Carbonate Crystalline Composites as a Biocatalyst. *Green Chem.* **2012**, *14* (8), 2216.

DOI: 10.1021/acsami.7b08147
ACS Appl. Mater. Interfaces 2017, 9, 21949−21958